J Fluoresc (2015) 25:1855–1866
DOI 10.1007/s10895-015-1678-y

ORIGINAL ARTICLE

A New Fluorescence Sensor for Cerium (III) Ion Using Glycine Dithiocarbamate Capped Manganese Doped ZnS Quantum Dots

Mohammad Kazem Rofouei[1] · **Narjes Tajarrod**[1] · **Majid Masteri-Farahani**[1] · **Reza Zadmard**[2]

Received: 14 June 2015 / Accepted: 28 September 2015 / Published online: 13 October 2015

Abstract A new fluorescence sensor for Ce^{3+}ions is reported in this paper. This sensor is based on the fluorescence quenching of glycine dithiocarbamate (GDTC)-functionalized manganese doped ZnS quantum dots (QDs) in the presence of Ce^{3+}ions. The synthesis of ultra-small GDTC-Mn:ZnS quantum dots (QDs) is based on the co-precipitation of nanoparticles in aqueous Solution. The nanoparticles are characterized with fluorescence spectroscopy, UV–vis absorption spectra, high-resolution transmission electron microscopy, X-ray power diffraction (XRD), and infrared spectroscopy. In the test carried out, it was found that the interaction between Ce^{3+}ions and GDTC capped Mn:ZnS QDs quenches the original fluorescence of QDs according to the Stern-Volmer equation and the results show the existence of collisional quenching process. A linear relationship was observed between the extent of quenching and the concentration of Ce^{3+}in the range of 2.0×10^{-6} to 3.2×10^{-5} mol.L^{-1}, with a detection limit of 2.29×10^{-7} mol.L^{-1}. The relative standard deviation of 1.61 % was obtained for five replicate measurements. The possible quenching mechanism was also examined by fluorescence and UV–vis absorption spectra. The interference of other cations was negligible on the quantitative determination of Ce^{3+}. This method proved to be simple, sensitive, low cost, and also reliable for practical applications.

Keywords Cerium (III) sensor · Fluorescence quenching · Nanosensor · Quantum dots · Glycine dithiocarbamate

Introduction

Quantum dots (QDs) are semiconductor nanocrystals composed of IIB-VIA groups (e.g., CdSe, CdTe, CdS and ZnSe) or IIIA-VA elements (e.g., InP and InAs) [1]. Due to the radius of QDs which is less than or equal to the excitation Bohr radius, they display unique optical, electrical,magnetic and catalytic properties which is defined as quantum confinement effect [2, 3]. Photophysical properties of QDs have inspired the researchers to use them as luminescent probes for detection of a variety of analytes, including many biological organic and inorganic species [4–7]. QDs have narrow and symmetric photoluminescence emission, with a Gaussian profile presenting a full-width-at-half-maximum of 25–35 nm. High quantum yields (QY≈0.2-0.9) brought brightness and a large physical cross-section that yielded strong one photon absorption ($\varepsilon\approx$ 104–106 M^{-1} cm^{-1}) and remarkably high two-photon absorption cross sections (σTPA≈103–104 GM) [8]. QDs' analytical performance is superior to common organic fluorophores due to their better chemical and photoluminescence stability, and upper optical properties. The optical properties of QDs are controlled by constituent materials in synthesis of homogeneous and stable quantum dots. Most QDs contain toxic heavy-metal elements such as Cd, Hg, Pb, etc. ZnS is one of the first discovered semiconductors, which promises for novel diverse applications, including light-emitting diodes (LEDs), electroluminescence, flat panel displays, infrared windows, sensors, lasers, bio devices, etc. Doping ZnS with ions such as manganese [9],copper [10], silver [8] or europium [11] results in a strong and characteristic luminescence, with high intensity and narrow emission band. Mn:ZnS nanocrystals are prepared extensively

✉ Mohammad Kazem Rofouei
rofouei@khu.ac.ir

[1] Faculty of Chemistry, Kharazmi University, Tehran, Iran

[2] Chemistry and Chemical Engineering Research Center of Iran, Tehran, Iran

by a chemical precipitation method in a homogeneous liquid phase reaction [9, 12–14].

Among rare earth elements, Ce^{3+} is the most widely distributed in the earth's crust [15–17]. Cerium is widely used in luminescence, agriculture, catalysis, nuclear energy, metallurgy, microelectronics, therapeutic application, magnetism, glass and ceramics, This wide-ranging usage encouraged researchers to study its environmental, medical and biological effects [18–20]. Different instrumental methods, including X-ray fluorescence [21], inductively coupled plasma (ICP-OES) [22, 23], spectrophotometry [24], spectrofluorometric [25, 26], ion-selective electrodes [27, 28] and potentiometric sensors [15] are used to determine Ce^{3+}cations. All these methods have advantages and disadvantages. Disadvantages include high consumption of energy and reagent, high costs method, disposal of harmful chemicals in the environment and the fact that some of the applied techniques suffer from lack of repeatability. In fluorimetry determination of trace Ce^{3+} two direct and indirect methods are adopted [26]. It is reported that direct method is the most sensitive one [29], for example, interference of coexisting ions, especially some rare earth's ions, Fe(III) and phosphate ions, always confront the direct methods.

In this work, we have used glycine dithiocarbamate (GDTC) as a new capping agent for synthesis of GDTC functionalized Mn:ZnS QDs by chemical co-precipitation method. GDTC as a ligand stabilizes surface of QDs and since such a bidentate chelating group, displays high affinity to QDs, it enhances QDs stability and improves resistance of QDs to photooxidation. The objective of this study is to develop a sensitive and selective method for detection of Ce^{3+} ions. Compared to most of the existing sensors for Ce^{3+}, this newly developed method has many advantages, including simplicity, low cost, high flexibility, less toxicity and good sensitivity.

Experimental

Reagents and Materials

Analytical reagent grade sodium sulfide (Na_2S-$9H_2O$), glycine, CS_2, zinc and manganese nitrate salts, and other cations used (all from Merck) were of the highest purity available and used without any further purification. All solutions were prepared using double distilled water (DDW).

Instrumentation

All fluorescence spectra were recorded on a JASCO fluorescence spectrophotometer (FP8500). The UV–vis absorption spectra of the Mn:ZnS QDs were also recorded using a Perkin–Elmer Lambda 25 spectrophotometer, using two matched 10-mm quartz cells. IR spectra were recorded using Perkin–Elmer RXI spectrometer with KBr disks. A digital pH meter, Metrohm model 692, equipped with a combined glass calomel electrode was employed pH adjustments. The morphology of the synthesized Mn doped ZnS QDs was examined using a Philips CM120 transmission electron microscope (TEM). The X-ray diffraction (XRD) pattern was obtained using France Intel (EQuinox 3000) Diffractometer with Cu $K_\propto$ source (λ=1.5406 A).

Synthesis of Glycine Dithiocarbamate (GDTC)

The literature is replete with many commercially available monothiols which are used in water [30]. In this experimental research glycine dithiocarbamate was used as a dithiol ligand by a simple mixture of glycine and carbon disulfide. GDTC was synthesized according to the aforementioned methods by some modification [31]. Briefly 2 mmol glycine was dissolved in 25 mL DDW and was reacted with 25 mL of an aqueous solution of NaOH (4 mmol). Afterwards, the suspension was stirred until a clear solution was obtained and consequently 2 mmol CS_2 was added dropwise. Finally, the mixture was stirred magnetically for 4 hours at room temperature. The formed GDTC was water soluble and showed UV absorption at 255 and 285 nm (Fig. 1). Furthermore the ^1H NMR spectrum of GDTC showed key protons (i.e., $-C-^{H_2}$) at 3.97 ppm [32].

Preparation of GDTC Coated ZnS:Mn QDs

The synthesis procedure is schematically shown in Scheme 1a and b. The Mn doped zinc sulfide nanocrystals were synthesized by a chemical co-precipitation method similar to that reported in the literatures with some modification [9, 33, 34]. For ZnS:Mn QDs synthesis, a 46.0 mL aqueous solution of 0.01 mol L^{-1} zinc nitrate with 4.0 mL of manganese nitrate (0.01 mol L^{-1}) was prepared in double distillated water. The solution was then transferred to a three-necked flask with continuous magnetic stirring

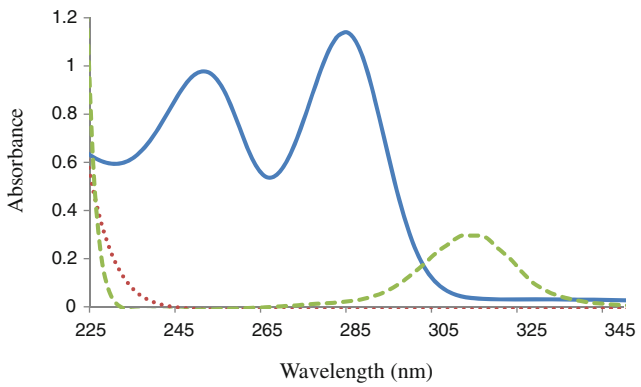

Fig. 1 UV spectra of GDTC (0.08 mol/L, solid line) compared with glycine (0.08 mol/L, dot line) and carbon disulfide (saturated solution, dash line) both dissolved in DDW

Scheme 1 Scheme for the preparation of GDTC (**a**) and GDTC-QDs conjugation (**b**)

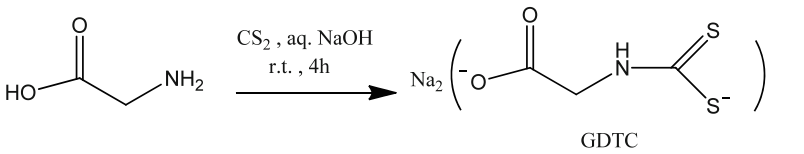

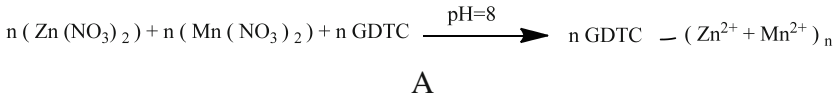

A

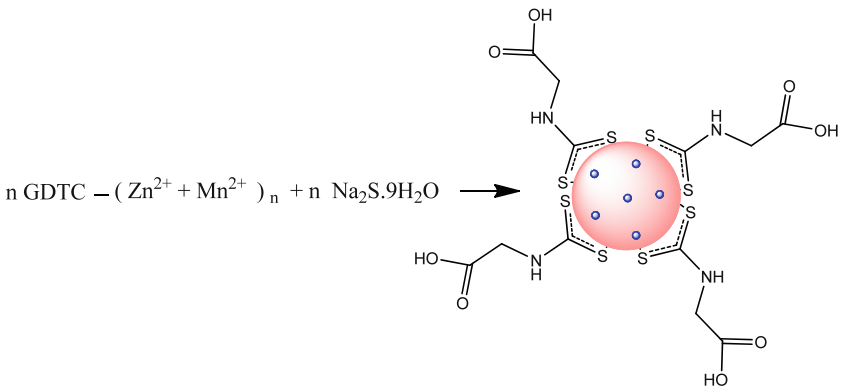

B

while N_2 gas was being inserted. Afterward, 50.0 mL aqueous solution of the capping agent (i.e., GDTC) was added drop wise to the solution under vigorous stirring at room temperature. After adjusting pH to 8, 50.0 mL aqueous solution of 0.01 mol L^{-1} sodium sulfide was added drop wise to the solution. The reaction was completed for 2 h and the colloid was refluxed for a fixed time to enhance the growth of the ZnS QDs. In the next step, the mixture was cooled down in room temperature gradually and the precipitated nanoparticles of ZnS:Mn were separated in a centrifuge with 6000 rpm within 15–20 minutes. Afterward the precipitants were washed 3 times with ethanol and finally were dried in vacuum at room temperature, yielding a fine powder.

Procedure for Spectrofluorometric Detection of Cerium (III)

In the first step, 50 mg.L^{-1} GDTC capped Mn-ZnS nanoparticle solution was suspended into a pH 7.5 Phosphate buffer saline (PBS). A known concentration of Ce^{3+} solution was added into Mn-ZnS nanoparticles solution and mixed thoroughly. For the quenching studies, 2.5 mL of ABS was poured into a in the quartz cell and 50 mg.L^{-1} of QDs with desired concentrations was added to the solution. Afterward, the solution was titrated by successive addition of 50 μL portions of 1.0×10^{-5} μg mL^{-1} stock solution of cerium ions and the solution was mixed before any fluorescence measurement. The fluorescence spectra of Mn:ZnS QDs in the absence and presence of the cerium (III) ion were recorded. The fluorescent intensity of the solution was recorded at excitation wavelength of 300 nm, and emission wavelengths of 575 nm.

Results and Discussions

Characterization of GDTC-capped Mn:ZnS

UV–vis and Fluorescence Study of GDTC-capped Mn:ZnS

The GDTC-capped Mn:ZnS QDs were characterized by UV–vis absorption spectroscopy and fluorimetry. The absorption spectra of GDTC-capped Mn:ZnS are shown in Fig. 2.

The absorption peak occurred at 300 nm. The band-slits of both excitation and emission were set at 5 nm and the scan speed was 1200 nm min^{-1}. In the corresponding fluorescence spectrum of Mn:ZnS QDs (Fig. 2), two emission bands at 415 nm and 575 nm were observed when excitation wavelength was set to 300 nm. The emission emerged at 415 nm originated from the defect-related emission of the ZnS and emission peak at wavelength of 575 nm, was generated by the transition from the triplet state ($^4T_1$) to the ground state

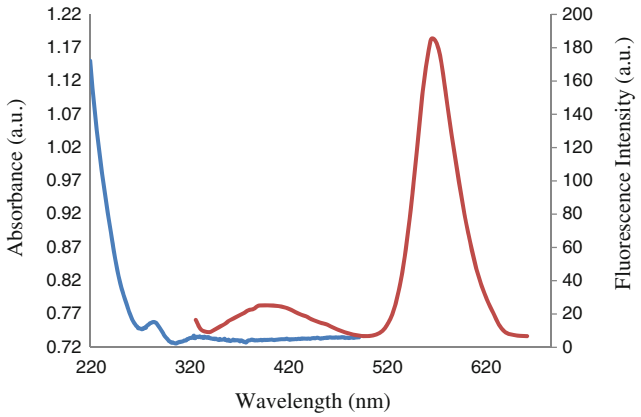

Fig. 2 **a** UV–vis absorption and **b** fluorescence spectra of synthesized Mn:ZnS QDs (60 mg/L)

($^6A_1$) of the Mn^{2+} incorporated into the ZnS host lattice. When Mn^{2+} ions were binded into the ZnS lattice the hybrid between the s-p electrons of the host ZnS and the d electrons of Mn^{2+} makes the forbidden transition of $^4T_1(G)$-$^6A_1(S)$ partially allowed. As a result, the yellow-orange PL was originated from the transition between the excited state and the ground state of the Mn^{2+} ion within a nanocrystalline ZnS lattice. By comparing the results of these studies, it was concluded that Mn^{2+} ions in our sample were indeed incorporated into the host ZnS nanocrystals [35–37]. It was observed that with systematic variation of molarity of the added capping agent, the optical band gap could be varied from a bulk value of 3.68–4.50 eV for clusters [38]. Therefore, in this study the concentration of GDTC was kept at fixed concentration of 2 mmol /200 mL total volume). One of the fundamental properties of semiconductors is the band gap - the energy separation between the filled valence band and the empty conduction band. In crystalline semiconductors, the following equation has been obtained to relate the absorption coefficient to incident photon energy [39]:

$$\alpha(\upsilon)h\upsilon = B\left(h\upsilon - E_{gap}\right)^m \quad (1)$$

Where E_{gap}, B, and $h\upsilon$ are the optical gap, constant, and incident photon energy, respectively; $\alpha(\upsilon)$ is the absorption coefficient defined by the Beer-Lambert's law. m is a constant equal to 1/2 for direct gap semiconductors and 2 for indirect gap semiconductors [40]. With some modifications [41], the value of band gap, in electron volt, can be calculated from the parameter λ_g by extrapolating the linear of the $(Abs\ (\lambda)\ /\lambda)^{1/m}$ vs. $1/\lambda$ curve at $(Abs(\lambda)/\lambda)^{1/m}=0$, which λ_g is related to E_{gap}, by the formula $E_{gap}=1239.83\ /\ \lambda_g$. By using the least squares technique, it was observed that the best fitting occurs for $m=1/2$. Extrapolating the straight-line portion of the plot shown in Fig. 3 to zero $(Abs(\lambda)/\lambda)^2$ gives the corresponding E_{gap} $(eV)=4.96$ value.

The quantum confinement effect allows one to tune the optical properties of nanoparticles by tuning it to the crystallite size. The crystallite size is given as follows:

$$r(E) = \frac{0.32-2.9\sqrt{E-3.49}}{2(3.50-E)} \quad (2)$$

Where $r(E)$ is particle radius and E is band gap in electronvolts [12]. Therefore, the average size of Mn:ZnS QDs was estimated to be 2.7 nm. The absorption peak of nanoparticles was blue shifted as compared to 345 nm (3.6 eV) of bulk ZnS. This large blue shift could be attributed to the combined effect of optical transition to the excitonic state of Mn:ZnS nanoparticles. Since the optical properties of QDs are generally due to quantum confinement effects, the UV–vis study indicates that the size of prepared particles is less than 10 nm [12, 42]. On the other hand, based on these observations, the high potential and suitability of GDTC make it an efficient capping agent to decrease the particle size from macro scale to nanometer scale through the precipitation synthetic method.

TEM Images of Quantum Dots

The morphology of the prepared GDTC capped Mn:ZnS nanoparticles was studied by transmission of electron microscopy (TEM). Figure 4 shows a typical image for the GDTC capped Mn:ZnS nanoparticles. The shape of these nanoparticles is dispersed sphere-like and the size of the particles seems are under 5 nm in diameter.

Some large particles are also apparent in the (Fig. 4), indicating aggregation of QDs. These aggregates may be formed at relatively high QD concentrations during the solvent evaporation process of TEM experiments.

X-ray Diffraction

The XRD pattern of the GDTC-capped Mn:ZnS nanoparticles was recorded and is shown in Fig. 5.

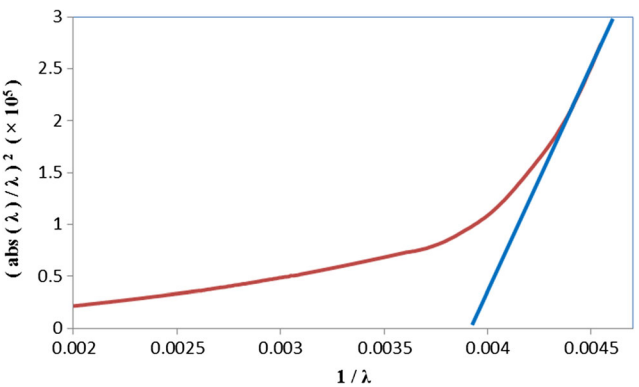

Fig. 3 Plot of $(Abs(\lambda)/\lambda)^2$ vs. $1/\lambda$ of Mn:ZnS nanoparticles

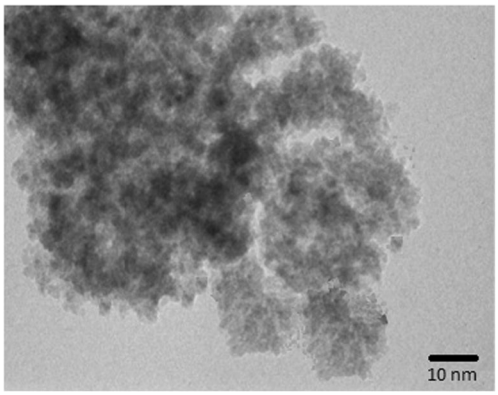

Fig. 4 TEM image of GDTC capped Mn:ZnS QDs

It could be seen that the synthesized particle has exhibited a cubic structure with peaks indexed as (1 1 1), (2 2 0), and (3 1 1) planes. No hexagonal (wurtzite) ZnS peak or impurity peak was detected in the XRD pattern [43]. This indicates that the Mn^{2+} ions substituted in Zn^{2+} sites cause no phase change in the crystal structure. The broadening of diffraction peaks confirmed that the crystallites were nano-sized. The crystallite size was calculated using Debye Scherrer's formula:

$$D = 0.9\lambda/\beta\cos\theta \quad (3)$$

Where D is the crystallite size, λ is the wavelength of X-rays, β is the full-width at half-maximum (FWHM) in radians, and θ is the diffraction angle The calculated particle size of the major XRD peak, using the FWHM, was 3.1 nm for GDTC-capped Mn:ZnS nanoparticle [44].

FT-IR Study

To verify the success of the synthesis of GDTC ligand and capping process, FT-IR measurements have been carried out. FT–IR spectroscopy gave qualitative information about the way in which the adsorbed surfactant molecules are bound to the surface of Mn:ZnS nanoparticles. Figure 6 shows FT–IR spectra of the GDTC (a) and GDTC capped Mn:ZnS (b).

The GDTC exhibit a number of characteristic bands [32]. The broad band at 3358 cm^{-1} is due to the overlap of stretching modes of ν (N-H) and ν (O-H) groups of water molecules. For carboxylic group, two bands were recorded at 1595 cm^{-1} (antisymmetric ν (COO^-) mode) and 1483 cm^{-1} (symmetric ν (COO^-) mode). The band shown at 1091 cm^{-1} is assigned to the $\nu_{C—N}$ modes corresponding to the bond between the dithiocarbamate carbon atom (C_1-N), (see labeling of the carbon atoms in Fig. 6a) and the amino acid nitrogen atom, and another corresponding to the ν(C_2-N) mode. These bands are recorded in 1091 cm^{-1}. Two bands that can be ascribed to the C-S stretching modes are recorded in 1003 $cm^{-1}$for antisymmetric and 587 cm^{-1} for symmetric modes [45]. There are coexisting IR absorption bands of –COO^-, and –NH observed on GDTC capped Mn:ZnS QDs. Therefore, carboxylic acid and amino group are present on the surface of the Mn:ZnS QDs, while the C–S group vibration (935 cm^{-1} and 587 cm^{-1}) is absent on the surface of the GDTC capped Mn:ZnS QDs. The reason for disappearance of C–S group vibration on the surface of Mn:ZnS nanoparticles is formation of covalent bonds between thiol side of GDTC and the surface of Mn:ZnS.

Effect of pH on Fluorescence Intensity

Generally, pH is one of the major variables that affect the fluorescence of QDs [25]. QDs are sensitive to their surrounding chemicals such as acids, bases, metallic ions, and biomolecules like proteins. QDs PL intensity could be directly correlated with pH values because QDs fluorescence is, in general, enhanced in basic medium and quenched in the acidic one [46, 47]. Therefore, the effect of pH on the fluorescence intensity of Ce^{3+}-GDTC capped Mn:ZnS QDs system was

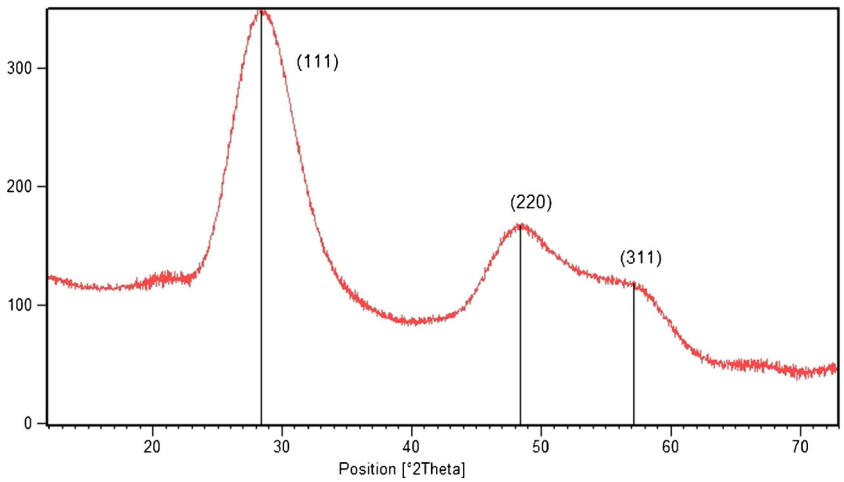

Fig. 5 The XRD pattern of prepared Mn:ZnS nanocrystals

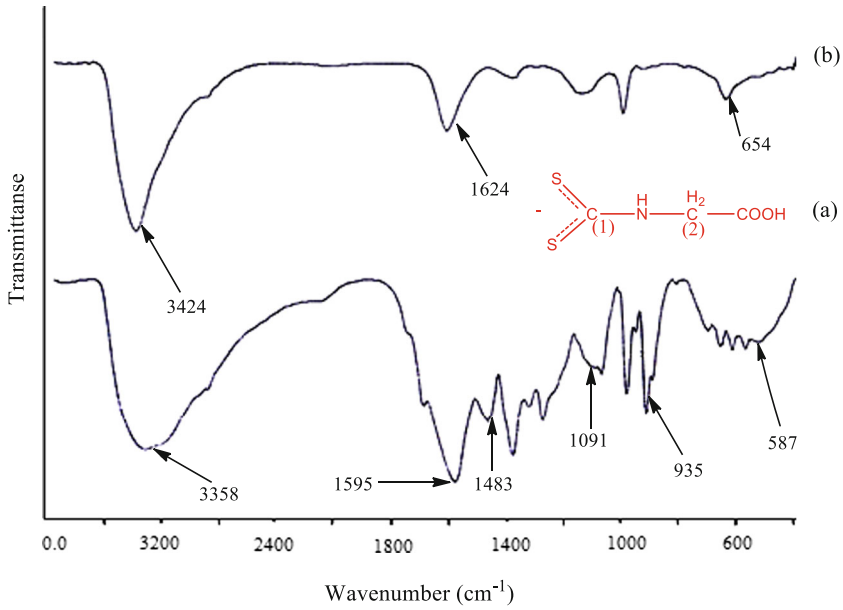

Fig. 6 FT-IR spectra of **a** free GDTC and **b** GDTC capped Mn:ZnS QDs

studied to obtain the optimum pH to develop a sensitive fluorescence sensor for Ce^{3+} ion. Figure 7 shows the effect of the pH on the fluorescence intensity of Mn:ZnS QDs after addition of Ce^{3+} ion. The fluorescence intensity was studied against pH in the range between 1.0 and 9.0 in order to obtain the optimum conditions for determination of Ce^{3+} ion.

The optimum net fluorescence intensity was obtained in the pH range of 4.5 and 7.5. Therefore, an acetic acid buffer with pH of 7.5 was used for the determination of Ce^{3+} ion study. When pH increases, the deprotonation of carboxyl group in the GDTC on the surface of QDs may occur. This deprotonation may strengthen the covalent bond between Ce^{3+} and GDTC molecule. At higher pH (pH>7.5), the QDs fluorescence becomes stronger since the particle surface is well passivated, but the concentration of Ce^{3+} decreases because of the formation of $Ce(OH)_3$ [48, 49]. This leads to a decrease in the fluorescence intensity with an increase in pH. At higher pH (pH>8) the fluorescence intensity decreases due to the existence of OH^- groups on the surface of QDs which hinders the interaction between Ce^{3+} and QDs.

Effect of GDTC-capped Mn:ZnS QDs Concentration

The influence of GDTC-capped Mn:ZnS QDs concentration on fluorescence intensity was studied and is shown in Fig. 8.

Fluorescence intensity of the system was increased by increasing the concentration of Mn:ZnS QDs solution. In low concentration of QDs, the fluorescence intensity was also very low; this fact may sacrifice the linear range of Ce^{3+} detection. On the other hand, high concentration of Mn:ZnS nanoparticles may result in self-quenching of the QDs fluorescence [50]. Considering these factors, a concentration of 50 $mg.L^{-1}$ of GDTC capped Mn:ZnS solution was used for sensing purposes.

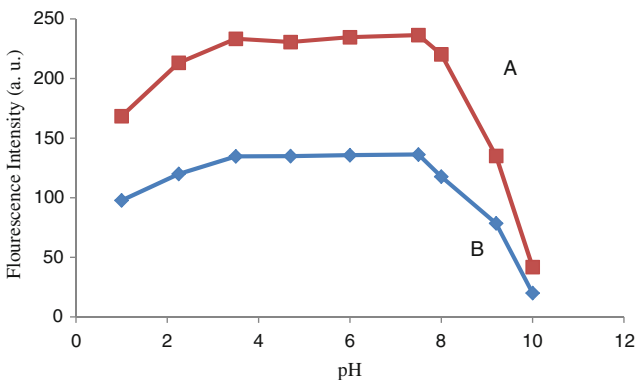

Fig. 7 Fluorescent intensity change of the system containing Mn:ZnS QDs (50 mgL^{-1}) and Ce^{3+} (5.0×10^{-5} mol L^{-1}) in different pH solutions

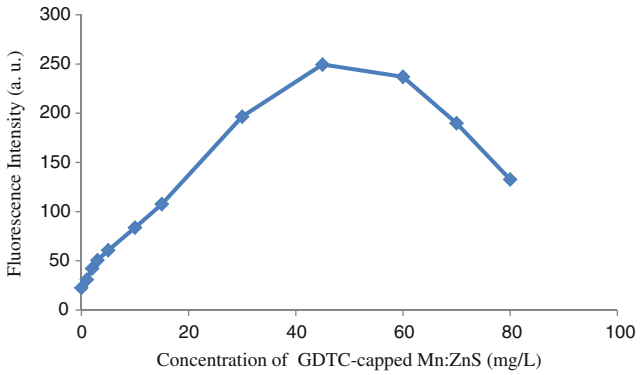

Fig. 8 Effect of colloidal Mn:ZnS QDs concentration on the fluorescence intensity (2.0 mL of PBS at pH=7.5, $[Ce^{3+}]=1.0\times10^{-5}$ mol L^{-1})

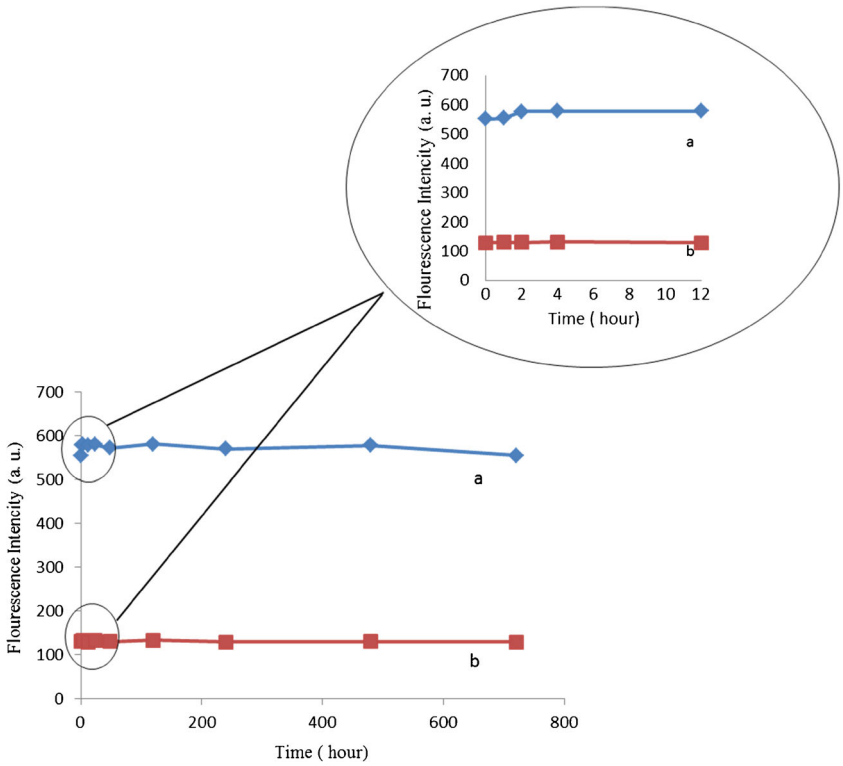

Fig. 9 **a** Fluorescence intensity change of 50 mgL^{-1} GDTC-capped Mn:ZnS per time **b** Effect of the time reaction under optimal conditions(pH=7.5,QDs concentration=50 mgL^{-1}, $[Ce^{3+}]=1.0\times10^{-5}$ $mol.L^{-1}$)

Stability of GDTC-capped Mn:ZnS QDs and Effect of Reaction Time

Usage of monothiol ligands causes QDs sensitivity to oxidation. This impediment was recently overcome by using dithiocarbamate moieties as ligands because of their ability in strong chelate-type binding to metal atoms. The resulting dithiocarbamate functionalized QDs exhibited improved resistance to photooxidation [51–53]. The stability of GDTC-capped Mn:ZnS was evaluated in aqueous solution at room temperature (Fig. 9a).

It was found that PL intensity gradually increases within 2 hours and then becomes stable, and the changes will be negligible up to 30 days. For investigation of reaction time, the fluorescence intensity of a typical mixture of GDTC-capped Mn:ZnS QDs and Ce^{3+} (5×10^{-5} mol L^{-1}) solution was studied under optimum conditions. As can be seen in Fig. 9b, the fluorescence signals remained constant without any significant change for more than 20 days.

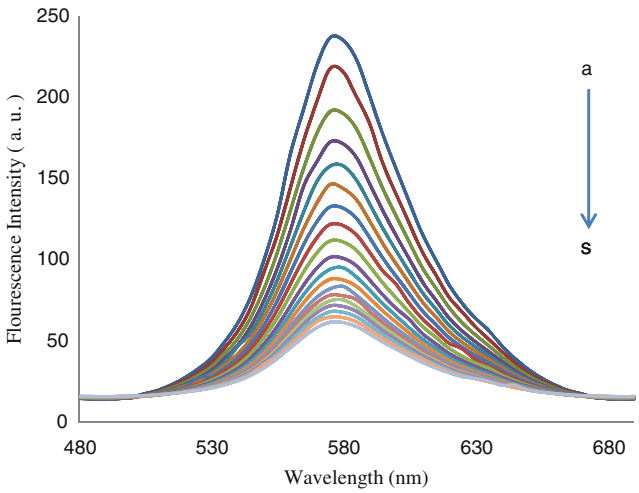

Fig. 10 Effect of the Ce^{3+} concentration (0.00-3.6×10^{-5} $mol.L^{-1}$, from (a) to (s)) on the fluorescence intensity of Mn:ZnS QDs (Conditions: 2.0 mL of PBS at pH=7.5, 50.0 mgL^{-1} of Mn:ZnS QDs)

Calibration Curves and Performance Characteristics

In order to achieve the sensitive detection of Ce^{3+}, the quenching study of GDTC-capped Mn:ZnS QDs by addition of Ce^{3+} ion was investigated at pH 7.5. Results showed that the

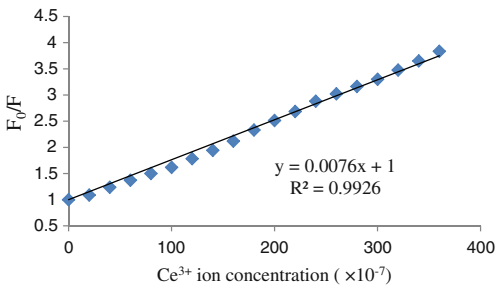

Fig. 11 Stern -Volmer plot of Ce^{3+} concentration dependence of the fluorescence intensity of QDs, with a 0.9981 correlation coefficient

Table 1 Comparison of the proposed method with some methods, reported in literature

System	pH	D.L(mol L^{-1})	L.R(mol L^{-1})	Ref.
ISE	3.5–10.0	7.6×10^{-6}	1.0×10^{-5}–1.0×10^{-1}	[16, 54]
	3.0–7.5	6.45×10^{-9}	2.0×10^{-8}–1.0×10^{-1}	
ICP-OES	6.0-9.0	7.13×10−7	–	[55]
Spectrophotometry	7.0–8.5	4.3×10^{-8}	1.4×10^{-9}–2.3×10^{-8}	[24]
Spectrofluorometric	7.6	9.4×10^{-4}	1×10^{-8}–1×10^{-4}	[29]
X-Ray fluorescence	8	2.6×10^{-6}	3.56×10^{-4}–5.7×10^{-4}	[21]
QD/ Fluorimetry	7.5	2.29×10^{-7}	2.0×10^{-6}–3.2×10^{-5}	This work

fluorescence intensity of Mn:ZnS nanoparticles decreased by increasing the Ce^{3+} ion concentration, immediately. The quenching effect of Ce^{3+} with different concentrations on PL intensity of Mn:ZnS QDs is presented in Fig. 10.

In the proposed system, Ce^{3+}gradually quenches the luminescence intensity of the Mn:ZnS QDs in a concentration dependence that was coincident with the fluorescence quenching described by Stern-Volmer equation.

$$F_0/F = 1 + K_{sv}[Q] \quad (4)$$

Where, F and F_0 are the luminescence intensities of the Mn-doped ZnS QDs at a given Ce^{3+} concentration and in a Ce^{3+} free solution, respectively. [Q] is the Ce^{3+} concentration and K_{sv} is the Stern-Volmer quenching constant. If the Stern-Volmer statement of binding of $Ce^{3+}$and nanocrystal is valid, plot of F_0/F as a function of [Q] should be linear.

As shown in Fig. 11, under the optimum conditions, there is a good linear relationship between the relative luminescence intensity (F_0/F) and the concentration of Ce^{3+}(C) in the range of 2.0×10^{-6} to 3.2×10^{-5} M Ce^{3+} with a correlation coefficient (R^2) of 0.9926.

Stern-Volmer quenching constant (K_{Sv}), which is a measurement of the quenching efficiency of the quencher, generally shows more sensitive system with a steeper slope and consequently a higher K_{Sv} value. K_{Sv} was calculated to be 9.2×10^4 L mol^{-1}. The limit of detection was evaluated using $3\sigma/S$, and it was found to be 2.29×10^{-7} mol L^{-1}, where σ is the standard deviation of the blank signal and S is the slope of the linear calibrated plot. The relative standard deviation of six replicate measurements for a solution containing 1.0×10^{-5} mol L^{-1} Ce^{3+} ion was 1.61 %. It was observed that the proposed method had a comparable or superior linear range and detection limit compared with the current sensors in use for Ce^{3+} detection. Analytical results of some of the techniques used for Ce^{3+} detection are summarized in Table 1.

Usually, fluorescence quenching of QDs is mainly based on electron transfer process, ion binding interaction, inner filter effect, and non-radiative recombination pathway [56, 57]. Typical Stern-Volmer quenching behavior happens by collisions between quencher (i.e., Ce^{3+}) and luminescent molecules (i.e., Mn:ZnS). Obviously, for both static and dynamic quenching, molecular contact between fluorophore and quencher is required. In this case, it is proposed that the quenching occurs as a result of coordination of $Ce^{3+}$and GDTC on the capping layer of the QDs [58]. In the following some reasons are presented.

a) The coordination changes the capping layer array and results in the reduction of fluorescence intensity, which is due to the high sensitivity to the capping layer of QDs. This hypothesis was evaluated by the fact that in high concentration of Ce^{3+}, precipitation is clearly visible, with low concentration of Ce^{3+} ions. As illustrated in Fig. 12, large particle sizes were observed which demonstrates that addition of Ce^{3+} indeed induces the aggregation of the Mn:ZnS QDs.
b) The UV–vis absorption spectra of The GDTC-capped Mn:ZnS QDs in the absence and the presence of Ce^{3+}ions were investigated. As shown in Fig. 13, no shift was observed in the absorption peak with addition of Ce^{3+} [59].
c) Since Ce^{3+} is a hard Lewis acid cation and has high tendency to make complexation with hard Lewis base ligands such as N donor atoms, a strong tendency of the complex at ion bonding between GDTC and $Ce^{3+}$is expected [60, 61].
d) It is suggested by some researchers that quenching can take place because of displacement of Zn in ZnS by heavy metal ions [62, 63]. N. Shanmugam et al.[64] reported a

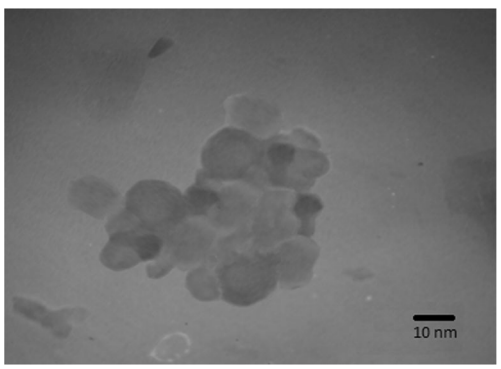

Fig. 12 TEM image of aggregated QDs in the presence of Ce^{3+}

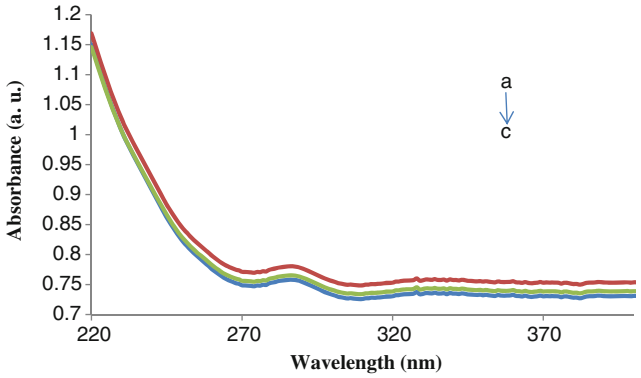

Fig. 13 UV–vis absorption spectra of ZnS QDs in the absence and presence of different concentrations of Ce^{3+}([Ce^{3+}] from a to c is 0,2,4 respectively μ mol.L^{-1})

blue shift in fluorescence spectra when Ce^{3+} is incorporated into ZnS structure,while authors' investigation of fluorescent quenching characteristics of this sensor showed no significant shift in emission wavelength (emission band centered at 415 nm) with increasing concentration of Ce^{3+} ions. It could be concluded that Ce^{3+} has not adsorbed on the surface of QDs.

e) Inner filter effect is one of the other fluorescence quenching reasons [62] which was investigated by the absorption spectrum of the Ce^{3+}-GDTC complex. As shown in Fig. 14 the absorption spectrum of Ce^{3+}-GDTC has not overlapped the emission spectrum of the QDs. The inner filter effect was thus dismissed.

Effect of Different Metal Ions on Luminescence Intensity

The effect of various ions on the fluorescence spectrum of Mn:ZnS QDs was also investigated by fluorescence titration of GDTC-capped Mn:ZnS QDs with some interfering ions. The study was done with three different ratios including 1:1, 1:10, and 1:100 (Ce^{3+}ion: interference ion) and the results are presented in Table 2.

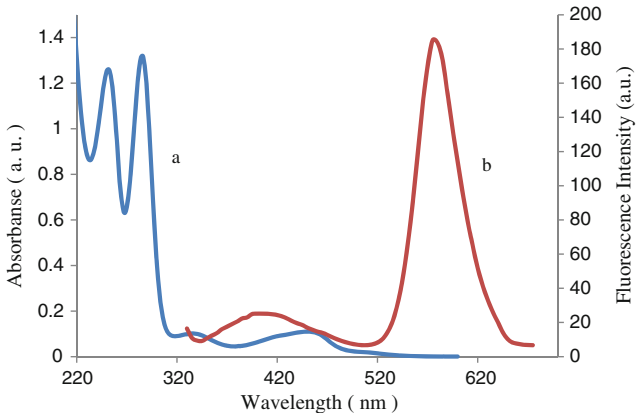

Fig. 14 Absorption spectrum of GDTC- Ce^{3+}complex (**a**) and emission spectrum of GDTC–QDs conjugate (**b**)

Table 2 Interfering effect of other ions: the concentration of GDTC-capped ZnS QDs is 50 mgL^{-1} and [Ce^{3+}]=1.0×10^{-5} mol L^{-1}

Interfering ion	Change of fluorescence intensity (%) Interfering ratio (Ce^{3+}ion / interfering ion)		
	1:1	1:100	1:1000
Ag^{+}	−0.66	−0.82	−1.69
Co^{3+}	+0.24	+0.27	+1.01
Cr^{3+}	+0.15	+0.21	+0.63
Cu^{2+}	−0.75	−0.84	−1.72
Hg^{2+}	−0.20	−0.29	−0.37
Pb^{2+}	+0.18	+0.27	+0.67
Ru^{3+}	+0.41	+0.52	+1.15
Fe^{3+}	−0.31	−0.39	−1.12
Cd^{2+}	+0.23	+0.28	+0.95
Sm^{3+}	−0.28	−0.33	−1.07
La^{3+}	+0.61	+0.73	+1.55
Eu^{3+}	−0.65	−0.73	−1.58
Pd^{2+}	−0.22	−0.30	−0.9
Ni^{2+}	−0.27	−0.30	−1.05
Mn^{2+}	+0.45	+0.59	+1.22

It was found that none of the three investigated ratios showed any significant interference with metal ions except with Cu^{2+} and Ag^{+} ions. The presence of foreign ions in 1:1 and 1:10 ratios produced lower interference than the RSD value of 1.61 %. Thus, ions causing errors more than 1.61 % are considered interferers. Based on Table 2, it could be noted that, only Ag^{+} and Cu^{2+} at 1:100 ratio cause interference. However, those ions of high concentration could not coexist with Ce^{3+} and their existence did not interfere the fluorescence determination of Cerium ion.

Sample Analysis

To investigate the possibility of practical application, recovery experiment of Ce^{3+} ion was measured in the tap and

Table 3 Determination results of cerium (III) ion in two water samples under optimal conditions

Sample	Added (μM)	Found (μM)	Recovery (%)	RSD (%)[a]
Tap water	0	Not founded	–	–
	5.0	4.96	99.2 %	1.02 %
	10.0	9.93	99.3 %	1.36 %
Ground water	0	Not founded	–	–
	5.0	4.95	99 %	1.23 %
	10.0	9.90	99 %	1.09 %

[a] Average of four replicate measurements

groundwater samples (Table 3). The tap water was deposited over a night. The results for the luminescence determination of Cerium ion are presented in Table 3. For this purpose, the described spectrofluorometric method was applied for determination of Ce^{3+} using Mn:ZnS QDs as luminescence sensor, under optimal conditions. From Table 3, the recoveries were found to be 98.8–104.7 % with relative RSDs ranged from 1.1 % to 3.9 % with standard addition method. These values indicate that this method has remarkable accuracy and precision for quantitative determination of Ce^{3+} ion in the presence of excess amount of other ions which exist in real samples.

Conclusions

In this paper, a new method was developed and used successfully for determination of cerium (III) based on quenching of fluorescence intensity of GDTC-functionalized QDs in the presence of cerium ions. Characterizations of the synthesized Mn:ZnS nanoparticles were investigated with TEM, XRD, UV–vis, and fluorescence spectroscopy. XRD studies suggested a single metallurgical phase formation. The average crystallite size was about 3.1 nm.

To the best of our knowledge, this study is the first work that is based on the use of glycine dithiocarbamate capped Mn-doped ZnS QDs for chemical sensing. This technique showed superior detection limit of 2.29×10^{-7} mol.L^{-1} and excellent selectivity over other competitive cations because of the specific and strong affinity of Ce^{3+}-GDTC and unique properties of QDs. Under the optimum conditions, the calibration plot was linear within the concentration range of 2.0×10^{-6} to 3.2×10^{-5} mol.L^{-1}. Based on the results, the designed sensor could be used to detect Ce^{3+} ion with good sensitivity. Compared with organic fluorophores, GDTC-Mn:ZnS nanoparticles as fluorescence probe offer many merits, such as high sensitivity, simple preparation of the nanoparticles,simple analytical application, low cost, narrow emission spectra and good photochemical stability. A comparison between the figures of merits of this luminescent QD probe with those of the previously reported ones (Table 1) clearly reveals that this fluorescent sensor could be categorized among the best Ce^{3+} probe ever reported.

Acknowledgments The authors are thankful to the Chemistry and Chemical Engineering Research Center of Iran for providing departmental facilities.

References

1. Kuang H, Zhao Y, Ma W, Xu L, Wang L, Xu C (2011) Recent developments in analytical applications of quantum dots. Trends Anal Chem 30:1620–1636
2. Gill R, Zayats M, Willner I (2008) Semiconductor quantum dots for bioanalysis. Angew Chem Int Ed 40:7602–7625
3. Rossetti R, Nakahara S, Brus LE (1983) Quantum size effects in the redox potentials, resonance Raman spectra, and electronic spectra of CdS crystallites in aqueous solution. J Chem Phys 79:1086–1088
4. Callan JF, De Silva AP, Mulrooney RC, Mc Caughan B (2007) Luminescent sensing with quantum dots. J Fluoresc 3–4:257–262
5. Galian RE, Guardia M (2009) The use of quantum dots in organic chemistry. Trends Anal Chem 28:279–91
6. Freeman R, Willner I (2012) Optical molecular sensing with semiconductor quantum dots (QDs). Chem Soc Rev 41:4067–85
7. Thomas D, Lonappan L, Rajith L, Cyriac ST, Kumar KG (2013) Quantum Dots (QDs) Based Fluorescent Sensor for the Selective Determination of Nimesulide. J Fluoresc 3:473–478
8. Jian W, Zhuang J, Zhang D, Dai J, Yang W, Bai Y (2006) Synthesis of highly luminescent and photostable ZnS:Ag nanocrystals under microwave irradiation. Mater Chem Phys 99:494–7
9. Labiadh H, Chaabane TB, Piatkowski D, Mackowski S, Lalevée J, Ghanbaja J et al (2013) Aqueous route to color-tunable Mn-doped ZnS quantum dots. Mater Chem Phys 140:674–682
10. Khosravi AA, Kundu M, Jatwa L, Deshpande SK, Bhagwat UA, Sastry M et al (1995) Green luminescence from copper doped zinc sulphide quantum particles. Appl Phys Lett 67:2702–2704
11. Qu SC, Zhou WH, Liu FQ, Chen NF, Wang ZG, Pan HY et al (2002) Photoluminescence properties of Eu^{3+}-doped ZnS nanocrystals prepared in a water/methanol solution. Appl Phys Lett 80:3605–7
12. Suyver JF, Wuister SF, Kelly JJ, Meijerink A (2001) Synthesis and photoluminescence of nanocrystalline ZnS:Mn^{2+}. Nano Lett 1: 429–33
13. Ma X, Song J, Yu Z (2011) The light emission properties of ZnS: Mn nanoparticles. Thin Solid Films 519:5043–5045
14. Segets D, Komada S, Butz B, Spiecker E, Mori Y, Peukert W (2013) Quantitative evaluation of size selective precipitation of Mn-doped ZnS quantum dots by size distributions calculated from UV/Vis absorbance spectra. J Nanoparticle Res 15:1–13
15. Ali TA, Mohamed GG, Azzam EMS, Abd-elaal AA (2014) Thiol surfactant assembled on gold nanoparticles ion exchanger for screen-printed electrode fabrication Potentiometric determination of Ce(III) in environmental polluted samples. Sensors Actuators B Chem 191:192–203
16. Afkhami A, Madrakian T, Shirzadmehr A, Tabatabaee M, Bagheri H (2012) New Schiff base-carbon nanotube–nanosilica–ionic liquid as a high performance sensing material of a potentiometric sensor for nanomolar determination of cerium(III) ions. Sensors Actuators B Chem 174:237–44
17. Awual MR, Yaita T, Shiwaku H (2013) Design a novel optical adsorbent for simultaneous ultra-trace cerium (III) detection, sorption and recovery. Chem Eng J 228:327–35
18. Wang L, Yu Y, Huang X, Long Z, Cui D (2013) Toward greener comprehensive utilization of bastnaesite: Simultaneous recovery of cerium, fluorine, and thorium from bastnaesite leach liquor using HEH(EHP). Chem Eng J 215–216:162–167
19. Abhilash S, Sinha MK, Sinha BDP (2014) Extraction of lanthanum and cerium from Indian red mud. Int J Miner Process 127:70–73
20. Hirano S, Suzuki KT (1996) Exposure, metabolism, and toxicity of rare earths and related compounds. Environ Health Perspect 104: 85–95
21. Masi AN, Olsina RA (1993) Preconcentration and determination of Ce, La and Pr by X-ray fluorescence analysis, using Amberlite XAD resins loaded with 8-Quinolinol and 2-(2-(5 chloropyridylazo)-5-dimethylamino)-phenol. Talanta 40:931–934
22. Achilli M, Ciceri G, Ferraroli R, Heltai D, Martinotti W (1989) Determination of cerium, yttrium and thorium in environmental samples. Analyst 114:319–23

23. Ayranov M, Cobos J, Popa K, Rondinella VV (2009) Determination of REE, U, Th, Ba, and Zr in simulated hydrogeological leachates by ICP-AES after matrix solvent extraction. J Rare Earths 27:123–7
24. Amin AS, Moustafa MM, Issa RM (1997) A rapid, selective and sensitive spectrophotometric method for the determination of Ce(III) using some bisazophenyl-β-diketone derivatives. Talanta 44:311–317
25. Zhang T, Lu J, Ma J, Qiang Z (2008) Fluorescence spectroscopic characterization of DOM fractions isolated from a filtered river water after ozonation and catalytic ozonation. Chemosphere 71: 911–21
26. Meng JX, Wu HJ, Feng DX (2000) Fluorimetry determination of trace Ce^{3+} with EDTP. Spectrochim Acta A 56:1925–8
27. Rounaghi G, Zadeh Kakhki RM, Sadeghian H (2011) A new cerium (III) ion selective electrode based on 2,9-dihydroxy-1,10-diphenoxy-4,7-dithia decane, a novel synthetic ligand. Electrochim Acta 56:9756–9761
28. Gupta VK, Singh AK, Gupta B (2006) A cerium(III) selective polyvinyl chloride membrane sensor based on a Schiff base complex of N, N′-bis[2-(salicylideneamino)ethyl]ethane-1,2-diamine. Anal Chim Acta 575:198–204
29. Akseli A, Rakicioğlu Y (1996) Fluorimetric trace determination of cerium(III) with sodium triphosphate. Talanta 43:1983–1988
30. Zhang Y, Schnoes AM, Clapp AR (2010) Dithiocarbamates as Capping Ligands for Water-Soluble Quantum Dots. ACS Appl Mater Interfaces 2:3384–3395
31. Thirumaran S, Ramalingam K (2000) Mixed ligand complexes involving aminoacid dithiocarbamates, substituted phosphines and nickel(II). Transit Met Chem 25:60–62
32. Criado JJ, Carrasco A, Macias B, Salas JM, Medarde M, Castillo M (1989) New PtS4 chromophores of dithiocarbamates derived from α-amino acids: synthesis, characterization and thermal behaviour. Inorg Chim Acta 160:37–42
33. Rajabi HR, Shamsipur M, Khosravi AA, Khani O, Yousefi MH (2013) Selective spectrofluorimetric determination of sulfide ion using manganese doped ZnS quantum dots as luminescent probe. Spectrochim Acta A 107:256–62
34. Wu H, Fan Z (2012) Mn-doped ZnS quantum dots for the room-temperature phosphorescence detection of raceanisodamine hydrochloride and atropine sulfate in biological fluids. Spectrochim Acta A 90:131–134
35. Bhargava RN (1996) Doped nanocrystalline materials-Physics and applications. J Lumin 70:85–94
36. Cao J, Yang J, Zhang Y, Yang L, Wang Y, Wei M et al (2009) Optimized doping concentration of manganese in zinc sulfide nanoparticles for yellow-orange light emission. J Alloys Compd 486: 890–894
37. Ren Z, Yang H, Shen L, Han S (2008) Hydrothermal preparation and properties of nanocrystalline ZnS:Mn. J Mater Sci Mater Electron 19:1–4
38. Viswanath R, Bhojya Naik HS, Yashavanth Kumar GS, Prashanth Kumar PN, Harish KN, Prabhakara MC et al (2014) Synthesis and photoluminescence enhancement of PVA capped Mn^{2+} doped ZnS nanoparticles and observation of tunable dual emission: a new approach. Appl Surf Sci 301:126–33
39. Tauc J, Menth A (1972) States in the gap. J Non-Cryst Solids 8–10: 569–85
40. Chopra N, Mansingh A, Chadha GK (1990) Electrical, optical and structural properties of amorphous V_2O_5-TeO_2 blown films. J Non-Cryst Solids 126:194–201
41. Ghobadi N (2013) Band gap determination using absorption spectrum fitting procedure. Int Nano Lett 3:2
42. Mu J, Gu D, Xu Z (2005) Synthesis and stabilization of ZnS nanoparticles embedded in silica nanospheres. Appl Phys A 80:1425–1429
43. Kole AK, Tiwary CS, Kumbhakar P (2013) Room temperature synthesis of Mn^{2+} doped ZnS d-dots and observation of tunable dual emission: Effects of doping concentration, temperature, and ultraviolet light illumination. J Appl Phys 113:114308
44. Dong B, Cao L, Su G, Liu W (2012) Synthesis and characterization of Mn doped ZnS d-dots with controllable dual-color emissions. J Colloid Interface Sci 367:178–182
45. Criado JJ, Fernandez I, Macias B, Salas JM, Medarde M (1990) Novel chelates of Pd(II) dithiocarbamates. Spectroscopic studies and thermal behaviour. Inorg Chim Acta 174:67–75
46. Stewart MH, Susumu K, Mei BC, Medintz IL, Delehanty JB, Blanco-Canosa JB et al (2010) Multidentate Poly(ethylene glycol) ligands provide colloidal stability to semiconductor and metallic nanocrystals in extreme conditions. J Am Chem Soc 132:9804–9813
47. Geszke-Moritz M, Clavier G, Lulek J, Schneider R (2012) Copper- or manganese-doped ZnS quantum dots as fluorescent probes for detecting folic acid in aqueous media. J Lumin 132:987–91
48. Aldana J, Lavelle N, Wang Y, Peng X (2005) Size-dependent dissociation ph of thiolate ligands from cadmium chalcogenide nanocrystals. J Am Chem Soc 127:2496–2504
49. Gao M, Kirstein S, Möhwald H, Rogach AL, Kornowski A, Eychmüller A et al (1998) Strongly photoluminescent CdTe nanocrystals by proper surface modification. J Phys Chem B 102: 8360–8363
50. Koneswaran M, Narayanaswamy R (2009) l-Cysteine-capped ZnS quantum dots based fluorescence sensor for Cu^{2+} ion. Sensors Actuators B Chem 139:104–109
51. Wang J, Xu J, Goodman MD, Chen Y, Cai M, Shinar J et al (2008) A simple biphasic route to water soluble dithiocarbamate functionalized quantum dots. J Mater Chem 18:3270–4
52. Querner C, Reiss P, Bleuse J, Pron A (2004) Chelating ligands for nanocrystals' surface functionalization. J Am Chem Soc 126: 11574–11582
53. Aldana J, Wang YA, Peng X (2001) Photochemical instability of CdSe nanocrystals coated by hydrophilic thiols. J Am Chem Soc 12:8844–8850
54. Zamani HA, Ganjali MR, Adib M (2007) Construction of a highly selective PVC-based membrane sensor for Ce(III) ions. Sensors Actuators B Chem 120:545–550
55. Jain VK, Handa A, Sait SS, Shrivastav P, Agrawal YK (2001) Preconcentration, separation and trace determination of lanthanum(III), cerium(III), thorium(IV) and uranium(VI) on polymer supported o-vanillin semicarbazone. Anal Chim Acta 429:237–246
56. Wu P, Zhao T, Wang S, Hou X (2014) Semicondutor quantum dots-based metal ion probes. Nanoscale 6:43–64
57. Duan J, Jiang X, Ni S, Yang M, Zhan J (2011) Facile synthesis of N-acetyl-l-cysteine capped ZnS quantum dots as an eco-friendly fluorescence sensor for Hg^{2+}. Talanta 85:1738–1743
58. Zhang K, Guo J, Nie J, Du B, Xu D (2014) Ultrasensitive and selective detection of Cu2+ in aqueous solution with fluorescence enhanced CdSe quantum dots. Sensors Actuators B Chem 190: 279–287
59. Chen J, Gao Y, Guo C, Wu G, Chen Y, Lin B (2008) Facile synthesis of water-soluble and size-homogeneous cadmium selenide nanoparticles and their application as a long-wavelength fluorescent probe for detection of Hg(II) in aqueous solution. Spectrochim Acta Mol Biomol Spectros 69:572–579
60. Kobayashi S, Sugiura M, Kitagawa H, Lam WWL (2002) Rare-earth metal triflates in organic synthesis. Chem Rev 102:2227–2302
61. Pearson RG (1963) Hard and soft acids and bases. J Am Chem Soc 85:3533–3539
62. Cai ZX, Yang H, Zhang Y, Yan XP (2006) Preparation, characterization and evaluation of water-soluble l-cysteine-capped-CdS nanoparticles as fluorescence probe for detection of Hg(II) in aqueous solution. Anal Chim Acta 559:234–239

63. Shanmugam N, Cholan S, Viruthagiri G, Gobi R, Kannadasan N (2014) Synthesis and characterization of Ce^{3+}-doped flowerlike ZnS nanorods. Appl Nanosci 4:359–365

64. Wang J, Zhou X, Ma H, Tao G (2011) Diethyldithiocarbamate functionalized CdSe/CdS quantum dots as a fluorescent probe for copper ion detection. Spectrochim Acta Mol Biomol Spectros 81: 178–183